The Influence of Pantograph Aerodynamic Characteristics Caused by Its Shroud

Shuanbao Yao, Dilong Guo, and Guowei Yang

LHD of Institute of Mechanics, CAS, Beijing, China
ysbao566@163.com

Abstract. The current collection performance of pantograph plays an important role in safe operation of high-speed train. Research shows that pantograph aerodynamic characteristics have a great influence on the current collection of pantograph. It's an efficient method to install a suitable pantograph shroud to improve the pantograph aerodynamic performance. In this paper, for the real pantograph systems used on CRH380A and CRH380B, the influence of unsteady aerodynamic characteristics caused by different types of pantograph shrouds with a running speed of 350km/h has been studied with detached eddy simulation method. The results show that the wake field caused by pantograph has salient unsteady characteristics. Different designs of pantograph shroud largely affect the pantograph wake field and the lift, drag and side forces of the pantograph slide. Compared to pantograph without shroud, the pantograph with shroud owns a more complex wake field. Besides, the strength and shedding frequency of the detached eddy vary a lot. This phenomenon becomes more serious in the cross- wind condition. The drag of pantograph slide increases about 12.8% and the lift reduces about 13.5% thanks to the pantograph shroud in CRH380A, while the drag reduces about 7.4% and the lift increases about 100% due to the pantograph shroud used on CRH380B. In the end, the author gives the pantograph shroud aerodynamic optimization recommendations based on the research results.

Keywords: Pantograph shroud, unsteady aerodynamic characteristics, DES.

1 Introduction

It's very important for safe operation of high-speed train to have a good current-collection between pantograph and catenary. The current-collection quality will be affected seriously by the aerodynamic characteristics of pantograph when a train runs at a speed of over 200km/h. And the higher of the speed, the more serious of the influence. It's one of an efficient method to install a suitable pantograph shroud to improve the pantograph aerodynamic performance (C. Talotte 2000). However, few public references about the influence of aerodynamic performance of pantograph caused by pantograph shroud can be found at present. The most popular pantograph shrouds used in China are European-style (e.g. pantograph shroud used on ICE, TGV etc.) and Japanese-style (e.g. pantograph shroud used

Y.-Q. Ni and X.-W. Ye (Eds.): Proceedings of the 1st IWHIR, Vol. 2, LNEE 148, pp. 41–52.
springerlink.com

on Shinkansen series), both of which are designed to improve the aerodynamic performance (QIAN Lixin 2003). In this paper, for the real pantograph systems used on CRH380A and CRH380B, the author mainly focus on the effect of unsteady aerodynamic characteristics of a pantograph caused by its shroud when a train runs in the open air in conditions with and without cross-wind.

2 Computational Model and Domain

The computational models used in the article are the real pantograph system used on CRH380A and CRH380B, called model I and model II respectively. In order to give a more accurate simulation of the pantograph wake field, the insulator device is modeled too (Figure 1). The computational domain used in this paper is as follows: taking the height h that calculated from the base to the top of the pantograph as the characteristic length, the length of inflow direction is taken to be 10h; the length of outflow direction is taken to be 15h; both the left and right of width is 4h; and the height is taken to be 8h. And about 10 million Cartesian meshes are used in this article. All the calculations in this paper are completed on the high-performance computing platform that belongs to Institute of Mechanics, CAS. And it takes about 300 hours for each calculation condition to compute on 128 CPUs.

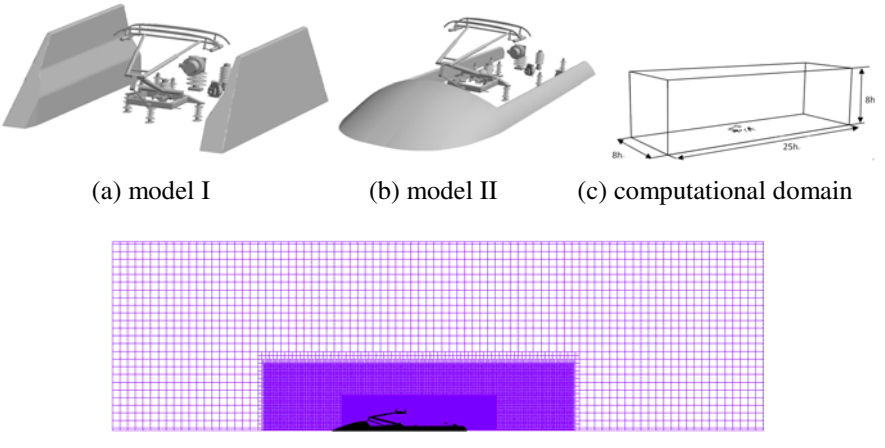

(a) model I (b) model II (c) computational domain

(d) distribution of mesh

Fig. 1 Calculation model, computational domain and distribution of meshes

3 Computational Algorithms

Since the unsteady aerodynamic characteristics of pantograph is a consequence of the flow field, it is crucial to understand the instantaneous flow in order to investigate its impact on the time varying aerodynamic forces. Thus, a time-dependent method, such as DNS, LES, DES and URANS, should be used to gain instantaneous information about the flow (Hassan Hemida and Siniša Krajnovic

2008). Direct numerical simulation requires simulating all scales of turbulence, so the minimum size of simulation should be less than the scale of dissipation area, which means that the minimum size of mesh should be less than the Kolmogorov scale (Zhaoshun Zhang *et al.* 2005). As a result, a great amount of mesh is required in order to get an accurate result for the DNS method, especially in the condition of high-Reynolds number, which cannot be achieved in engineering in the foreseeable future. A pure LES of an airborne or ground vehicle would use well over 10^{11}grid points and close to 10^7 time steps, which is estimated to be possible in 2045(Philippe R. Spalart 2000). The boundary layer dominates this expense and the resolution needs in the outer region of the boundary layer are firm, with at the least 20 points per thickness δ in each direction. URANS arises from a negative assessment of models and the relentless attempts to build into them first-principle content and rational ideas, so URANS models can be adjusted to predict boundary layers and their separation well, but not large separation regions. Detached-eddy simulation (DES) is proposed to resolve the problem of high-Reynolds number, massively separated flows, for which DES is convincingly more capable presently than either unsteady Reynolds-averaged Navies-Stokes (URANS) or large-eddy simulation (LES) (Philippe R. Spalart 2009). So DES will be used as the method of solution in this paper.

3.1 Method of DES

The DES model is a hybrid RANS/LES model which avoids the Reynolds-number restrictions of traditional LES by blending to a RANS-type model where the local mesh is too coarse to support calculations in LES model. Two types of DES are very popular: one is that based on the simple Spalart-Allmaras model, and the other is that based on the SST model, which will be used in this paper. The transport equations for k and w in the SST k-ω model are as follows:

$$\frac{\partial(\rho k)}{\partial t}+\frac{\partial}{\partial x_j}(\rho u_j k)=\frac{\partial}{\partial x_j}((\mu_t+\frac{\mu_t}{\sigma_k})\frac{\partial k}{\partial x_j})+P_k-\rho\beta' k\omega \tag{1a}$$

$$\frac{\partial(\rho\omega)}{\partial t}+\frac{\partial}{\partial x_j}(\rho u_j\omega)=\frac{\partial}{\partial x_j}\left((\mu_l+\frac{\mu_t}{\sigma_\omega})\frac{\partial\omega}{\partial x_j}\right)+\gamma\frac{\omega}{k}\cdot P_k-\rho\beta\omega^2+\frac{2\rho(1-F_1)\sigma_{\omega 2}}{\omega}\frac{\partial k}{\partial x_j}\frac{\partial\omega}{\partial x_j} \tag{1b}$$

F_1 will approach to 1 near the wall, and the model will close to the k-ω turbulence model. Far away from the wall, F1 will approach to 0 and the model will close to k-ε model. The constants appeared in the k-ω model are:

$$\sigma_{k1}=0.85\ ,\ \sigma_{\omega 1}=0.5\ ,\ \beta_1=0.075,\quad \beta^*=0.09,\quad \gamma_1=0.5532$$

For the k-ε model, the constants are:

$$\sigma_{k2}=1.0\ ,\ \sigma_{\omega 2}=0.856\ ,\ \beta_1=0.0828,\quad \beta^*=0.09,\quad \gamma_1=0.4404$$

F_1 takes a form as:

$$F_1=\tanh\left(\arg_1^4\right),\quad \arg_1=\min\left[\max\left(\arg_{1a},\arg_{1b}\right),\arg_{1c}\right]$$

$$\arg_{1a}=\sqrt{k}/\left(0.09\omega y\right),\quad \arg_{1b}=500\mu_l/\left(\bar{\rho}\omega y^2\right)$$

$$\arg_{1c} = 4\bar{\rho}k\sigma_{\omega 2} / \left(CD_{k\omega} y^2\right),\ CD_{k\omega} = \max\left(\frac{2\bar{\rho}\sigma_{\omega 2}}{\omega}\frac{\partial k}{\partial x_i}\frac{\partial \omega}{\partial x_i},\ 10^{-20}\right)$$

where μ_l is the dynamic viscosity of laminar flow, and the dynamic viscosity of turbulence flow μ_t can be obtained from the following function:

$$\mu_t = \min\left[\frac{\rho k}{\omega}, \frac{a_1 \rho k}{\Omega F_2}\right]$$

For the DES model, the equation (1b) takes the form as:

$$\frac{\partial(\rho k)}{\partial t} + \mu_j \frac{\partial(\rho k)}{\partial x_j} = \frac{\partial}{\partial x_j}((\mu_t + \frac{\mu_t}{\sigma_k})\frac{\partial k}{\partial x_j}) + P_k - \frac{\rho k^{1.5}}{l_{k-\omega}} \tag{2}$$

where $l_{k-\omega} = \frac{k^{0.5}}{\beta_k \omega}$ is a parameter to indicate the size of turbulence. For the DES model based on SST model, the value of $l_{k-\omega}$ should be decided by $\min(l_{k-\omega}, C_{DES}\Delta)$, where $\Delta = \max(\Delta x, \Delta y, \Delta z)$ is the largest length of every cell. $C_{DES} = (1 - F_1) C_{DES}^{k-\varepsilon} + F_1 C_{DES}^{k-\omega}$. The values of the constants $C_{DES}^{k-\varepsilon}$ and $C_{DES}^{k-\omega}$ are 0.61 and 0.78 respectively.

3.2 Details of Calculation

In this paper, finite volume method is chosen for spatial discretisation. Roe's FDS scheme is used to calculate convective fluxes, and second-order central difference is used to compute viscous fluxes. Besides, Lower-Upper Symmetric Gauss-Seidel (LU-SGS) is chose for temporal discretisation. In order to capture instantaneous information, physical time step is set to be 1e-4s and number of inner iterations is set to be 5.

4 Calculated Cases

Six cases are computed in this paper to illustrate the influence on unsteady aerodynamic performance of pantograph caused by pantograph shroud in conditions with and without cross-wind, and the details are shown as follows (Table 1):

Table 1 Details of cases used in this paper

Case number	Type of pantograph shroud	The speed of train(m/s)	The speed of cross-wind(m/s)
Case 1	No	97.22	0
Case 2	Model I	97.22	0
Case 3	Model II	97.22	0
Case 4	No	97.22	15
Case 5	Model I	97.22	15
Case 6	Model II	97.22	15

5 Results and Discussions

5.1 The Flow Around Pantograph without Cross-Wind

There are usually two installation methods of pantograph on high-speed train. One is that pantograph is installed against the flow; and the other is that pantograph is installed along the flow, which is considered in this article. Different installation methods will seriously affect aerodynamic characteristics of pantograph skateboard which is a key factor that has a great influence on the current collection performance of pantograph and will be mainly discussed in the next passages. When pantograph is installed against the flow, the aerodynamic lift of pantograph slide is usually a positive force, which will increase the contact force between pantograph and catenary. Otherwise, the aerodynamic lift of pantograph slide will turn negative force and decreased the contact force.

5.2 The Flow Structure of the Wake Field of Pantograph

Figure 2 shows that the flow structure of the wake field of pantograph is very complex. The wake field is full of numerous small vortices which are generated on the pantograph surface. These eddies detach from the surface and flow into the downstream in the wake flow. Some horseshoe vortices generate on the train surface and develop rapidly in the downstream and break down at last. The insulator device makes the wake field more complex due to amounts of disarray vortices which will have a serious effect on the aerodynamic force of pantograph slide, as shown in Figure 2(a). The wake field becomes more complex when the pantograph shroud is installed, as shown in Figure 2(b) and (c). Two vortices are generated on both sides of the pantograph shroud in case 2 and detach quickly from the shroud surface and extend to the wake field. These four vortices are steady and can make the wake field more disordered. The pantograph shroud in case 2 compresses the air and increases the speed of the air through the pantograph, so that the strength of eddies detaching from the shroud surface will increase a lot. Those detached eddies will keep a long time in the wake field before breaking down, as shown in Figure 2(b). Along with the pantograph shroud surface in case 3, the flow detaches on the edge of the shroud and lots of small eddies generate quickly near the root of the pantograph. These vortices combine with the vortices caused by pantograph and the strength of the combined eddies will increase largely, which may prevent them from break down, as shown in Figure 2(c).

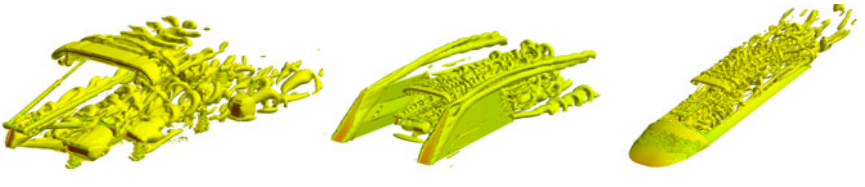

(a) case 1 (b) case 2 (c) case3

Fig. 2 Transient Q isosurface graph of case 1, case 2 and case 3 (Q=5000)

Some vortex streets generate from the upper part of the base of pantograph, as shown in Figure 3, 4 and 5. The vortex streets in case 2 and case 3 are more intense than that in case 1, which this will make the wake field more complex than that without pantograph shroud. Due to the complex wake field, the oscillation amplitude of aerodynamic force of pantograph slide will be very large, which has a bad effect on the current collection between pantograph and catenary. Figure 5 shows that air flows along with the pantograph shroud and separates at the edge, some detaches and evolves to small eddies as described in previous, and others flow over the upper part of the base and then go to the downstream of the wake field. This flow structure will increase the lift force of pantograph seriously.

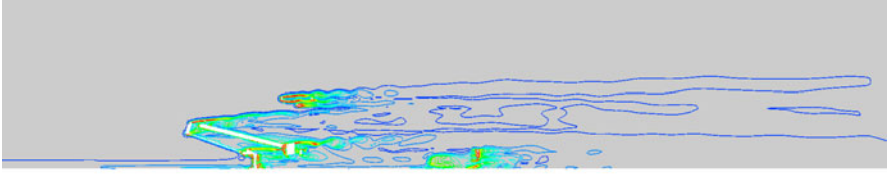

Fig. 3 Instantaneous vortices on the symmetry plane of case 1

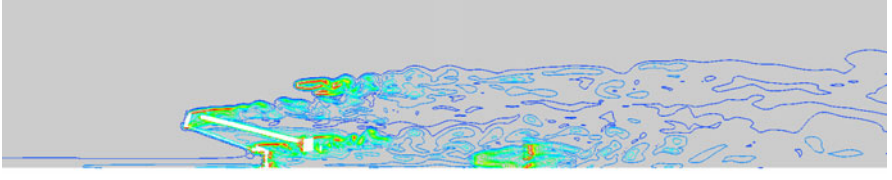

Fig. 4 Instantaneous vortices on the symmetry plane of case 2

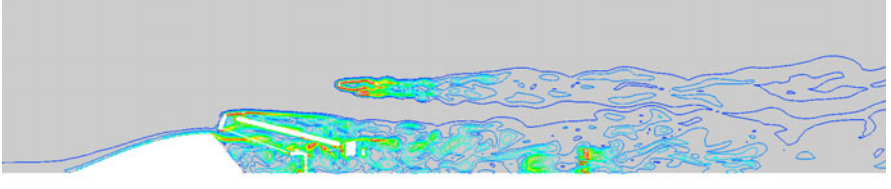

Fig. 5 Instantaneous vortices on the symmetry plane of case 3

5.3 The Force of Pantograph Slide

The mean drag of the slide is very large in all three cases, as shown in Table 2. But the fluctuation is not very serious in these cases; for case 1, the fluctuation is about 5.4%; for case 2, the value becomes to 13.4%; and for case 3, the value is 11.2%. Compared to case 1, the drag increases about 12.8% in case 2 and reduces about 7.9% in case 3. So the type of model II is useful to reduce the drag of

pantograph slide and model I has a bad effect on reducing the aerodynamic drag of the slide. The lift force of pantograph slide is a negative value because of the installation method discussed in the previous passages. The fluctuation of the lift force is very large in all three cases, especially in case 3. For case 1, the fluctuation is about 109.6%; for case 2, this value is 468.9%; and for case 3, the value is 132.7%. Compared to case 1, the absolute value of the mean lift force reduces about 13.5% in case 2 and increases about 100% in case 3. So model I can reduce the lift force of the pantograph slide, although it is mainly used to reduce the aerodynamic noise, and model II is not good for the slide to reduce the lift force. The side force of the slide is very small and can be neglected.

Table 2 Forces of pantograph slide without cross-wind

Force(N)		Case 1	Case 2	Case 3
Drag Force	Max	801	931	759
	Min	759	814	679
	Mean	774	873	717
Lift Force	Max	-23	59	-27
	Min	-80	-152	-165
	Mean	-52	-45	-104
Side Force	Max	0	6	1
	Min	-17	-10	-7
	Mean	-1	-2	-3

5.4 Time Domain and Frequency Domain Characteristics of the Lift of Pantograph Slide

The aerodynamic lift of pantograph slide has a great impact on the current collection between pantograph and catenary. So the influence of the unsteady aerodynamic lift characteristic of the slide caused by pantograph shroud will be mainly discussed in this section. Figure 6 shows that the oscillation period and amplitude of the lift is nearly stable, and two dominating peaks are found in the autopower spectra of the time varying signals of the lift force in case 1. The oscillation period and amplitude of the lift in case 2 is longer than that in case 1, and the oscillation period of the lift is not so distinguished, as shown in Figure 7 and 8. However, two dominating peaks can be found in both of the autopower spectra of the time varying signals of the lift in case 2 and case 3. But the corresponding St Number ($St = fD / U_{\infty}$, where f is the time-varying frequency of lift force) is different. For case 1, the dominating peaks are at the St=1.8, 2.05; for case 2, the dominating peaks are at the St=2, 2.4; and for case 3, the dominating peaks are at the St=1.8, 2.2. So the frequency of the oscillation of pantograph slide lift will increase when installing pantograph shroud like model I and model II in conditions without cross-wind.

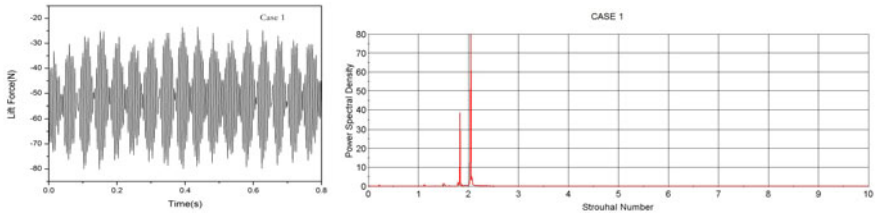

Fig. 6 Time history of lift force and power spectral density map of pantograph slide of case 1

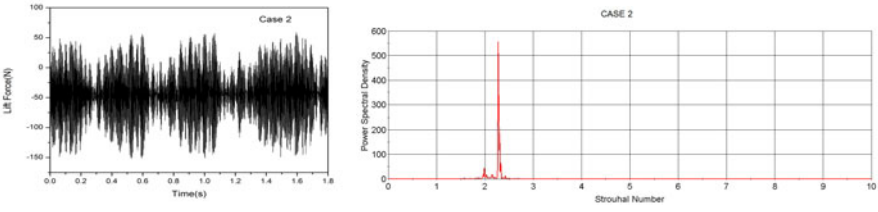

Fig. 7 Time history of lift force and power spectral density map of pantograph slide of case 2

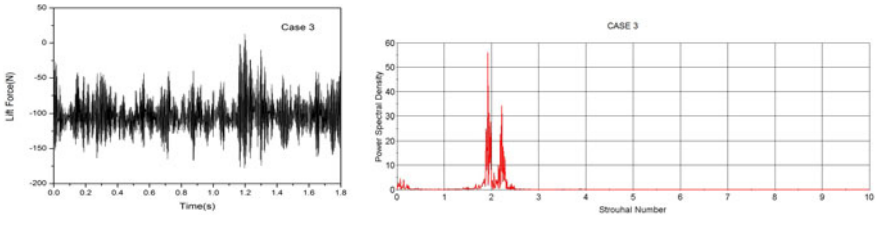

Fig. 8 Time history of lift force and power spectral density map of pantograph slide of case 3

6 The Flow Around Pantograph with Cross-Wind

6.1 The Flow Structure of the Wake Field of Pantograph

Pantograph experiences stronger aerodynamic forces when cruising in a strong cross-wind than that without cross-wind, which will seriously influence the current collection between pantograph and catenary. Compared to Figure 2, the wake field of pantograph is more complex and has significant non-symmetry characteristics in cross-wind condition, as shown in Figure 9, and this will largely increase the side force of pantograph. Some big vortices in the windward become stronger due to the influence of cross-wind than that without cross-wind. Figure 2(b) shows that the two steady vortices that are generated on the steeple of the shroud still exist but slope to leeward side, and the non-symmetry characteristic is not so obviously than that without shroud (Figure 9(a)). As a result, the side force of the slide in case 5 will be less than that in case 4. Compared to Figure 9(b),

there are more small vortices around the base of pantograph in Figure 9(c) and the non-symmetry characteristic is stronger. However, the non-symmetry characteristic in case 4 is stronger than that both in case 5 and case 6, so the shroud will have a good effect to improve the aerodynamic characteristics of pantograph in cross-wind condition.

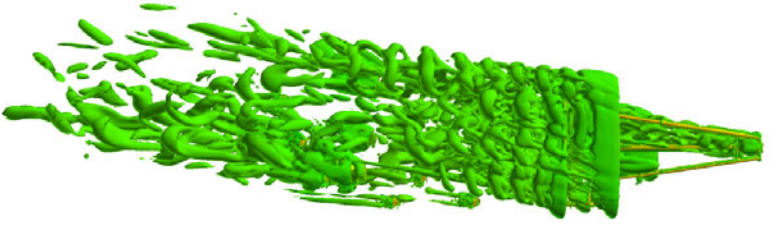

Fig. 9 (a) Transient Q isosurface graph of case 4 (Q=5000)

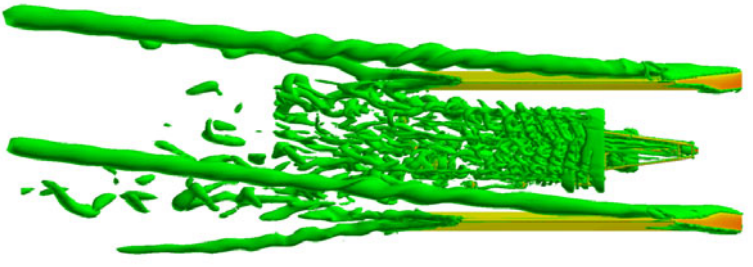

Fig. 9 (b) Transient Q isosurface graph of case 5 (Q=5000)

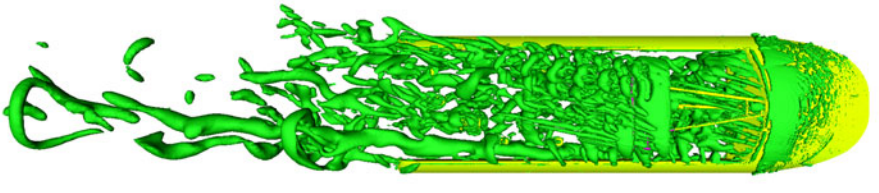

Fig. 9 (c) Transient Q isosurface graph of case 6 (Q=5000)

6.2 The Force of Pantograph Slide

Compared to Table 2, the absolute values of mean forces, except mean lift force of case 6, of pantograph slide with cross wind increase a lot in Table 3. The mean drag forces in case 4, case 5 and case 6 are larger than that in case1, case 2 and case 3 about 6.5%, 4.8% and 7.4%, respectively. And compared to case 4, the

mean drag force increases 11.0% in case 5 and reduces 6.6% in case 6. The fluctuations of lift force of pantograph slide change a lot in cross-wind condition with values of 187.1%, 188.1% and 97.1%, respectively. So model II can inhibit pantograph swing up and down efficiently. The absolute values of mean lift forces in the cases of Table 3 are larger than that in the cases of Table 2 about 19.2%, 86.7% and -0.9%, respectively. Compared to case 4, the absolute value of mean lift force increases 35.5% in case 5 and 66.1% in case 6. Side force of the slide increases largely with the cross-wind due to the non-symmetry characteristics of wake field, as shown in Table 3. The fluctuation of side force of the slide in case 4, case 5 and case 6 are 11.7%, 17.1% and 70.6%, respectively. Compared to case 4, the mean side force reduces 26.7% in case 5 and 9.6% in case 6. So a conclusion can be made that shroud has a positive influence on pantograph to reduce the side force of the slide, which will improve lateral stability of pantograph in cross-wind condition.

Table 3 Forces of pantograph slide with cross-wind (the speed is 15m/s)

Force(N)		Case 4	Case 5	Case 6
Drag Force	Max	881	965	804
	Min	781	861	739
	Mean	824	915	770
Lift Force	Max	-4	-3	-49
	Min	-120	-161	-149
	Mean	-62	-84	-103
Side Force	Max	99	76	128
	Min	88	64	68
	Mean	94	70	85

6.3 Time Domain and Frequency Domain Characteristics of the Lift of Pantograph Slide

Compared to Figure 6, time history of the lift force of pantograph slide changes a lot in cross-wind condition, as shown in Figure 10. Only one dominating peak at St=2.0 is found in the autopower spectra of the time varying signals of the lift force in case 4. For case 5, the oscillation period is also becomes larger than that in case 2 and one dominating peak at St=2.1 is found in Figure 11. For case 6, there is no apparent oscillation period of the lift force of the slide, and the amplitude of the lift is almost stable, as shown in Figure 12. One dominating peak can be found at St=1.9. So model I will increase the frequency of the oscillation of pantograph slide lift and model II will decrease the oscillation frequency in cross-wind condition.

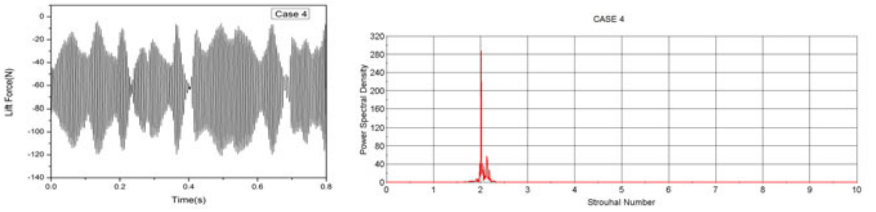

Fig. 10 Time history of lift force and power spectral density map of pantograph slide of case 4

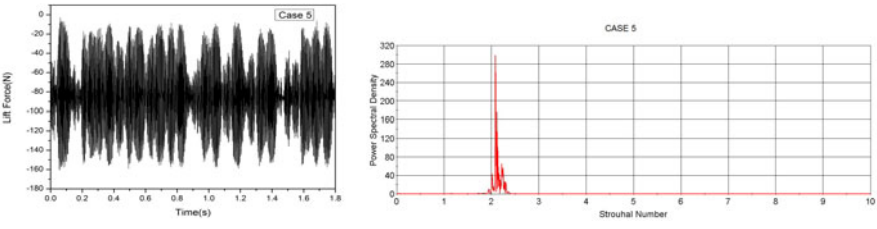

Fig. 11 Time history of lift force and power spectral density map of pantograph slide of case 5

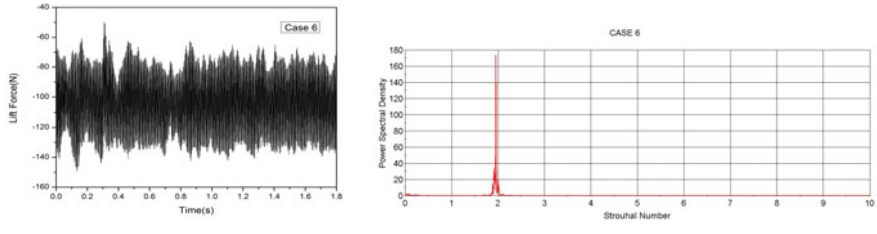

Fig. 12 Time history of lift force and power spectral density map of pantograph slide of case 6

7 Conclusions

Detached eddy simulations were performed on the flow around a pantograph to study the influence of pantograph aerodynamic characteristics caused by pantograph shroud. The flow field around pantograph shows seriously unsteady characteristics. Compared to pantograph without shroud, the wake field of the pantograph installing shroud becomes more complex and the strength and shedding frequency of the detached eddies change a lot, which will have a serious effect on the current collection of pantograph system, and this phenomenon becomes more seriously in cross-wind condition. Two dominating peaks that can be found in the autopower spectra of the time varying signals of pantograph slide lift force in conditions without cross-wind. However, the dominating peaks change

to one in cross-wind condition. Model I can reduce the absolute value of pantograph slide lift force and increase the drag force in conditions without cross-wind. Although model II can increase the lift of the slide, it will reduce the pantograph slide drag force in conditions with and without cross-wind. Both types of the shrouds have a positive effect to reduce the side force of the slide in cross-wind condition. Based on the above analysis, the pantograph shroud that composed of a baffle with half of height of the pantograph and a front spoiler is recommended to be installed on a high-speed train in order to improve the aerodynamic performance of pantograph.

Acknowledgments. This work was supported by 973 program under 2011CB 711100 and national key technology R&D program under 2009BAQG12A03. And Computing Facility for Computational Mechanics Institute of Mechanics, Chinese Academy of Sciences is gratefully acknowledged.

References

Talotte, C.: Aerodynamic noise: a critical survey. Journal of Sound and Vibration 231(3), 549–562 (2000)

Qian, L.X.: Recent Technical Development of High-speed Trains in the World. China Academic Journal Electronic Publishing House 24(4) (2003)

Hassan, H., Siniša, K.: LES Study of the Influence of a Train-Nose Shape on the Flow Structures Under Cross-Wind Conditions. Journal of Fluids Engineering 130(9) (2008)

Zhang, Z.S., Cui, G.X., Xu, C.X.: Theory and Modeling of Turbulence. Tsihghua University Press (2005)

Spalart, P.R.: Detached-Eddy Simulation. Annual Review of Fluid Mechanics 41, 181–202 (2009)

Spalart, P.R.: Strategies for turbulence modeling and simulations. Int. J. Heat Fluid Flow 21, 252–263 (2000)

Diedrichs, B.: Aerodynamic Calculations of Crosswind Stability of a High-speed Train Using Control Volumes of Arbitrary Polyhedral Shape. Bluff Bodies Aerodynamics & Applications (2008)

Kang, S., Iaccarino, G., Ham, F.: DNS of buoyancy-dominated turbulent flows on a bluff body using the immersed boundary method. Journal of Computational Physics 228, 3189–3208 (2009)

Galletti, B., Bottaro, A., Bruneau, C.H., Iollo, A.: Accurate model reduction of transient and forced wakes. European Journal of Mechanics B/Fluids 26, 354–366 (2007)

Khier, W., Breuer, M., Durst, F.: Flow structure around trains under side wind conditions: a numerical study. Computers & Fluids 29, 179–195 (2000)

Hemida, H., Baker, C.: Large-eddy simulation of the flow around a freight wagon subjected to a crosswind. Computers & Fluids 39, 1944–1956 (2010)

Diedrichs, B.: Aerodynamic crosswind stability of a regional train model. Journal of Rail and Rapid Transit. 224, 6580–6591 (2010)

Hemida, H., Krajnovic, S.: Transient Simulation of the Aerodynamic Response of a Double-Deck Bus in Gusty Winds. Journal of Fluids Engineering 131(3) (2009)